PROOF COPY 022212PHF

Nonlinear electrokinetic ejection and entrainment due to polarization at nearly insulated wedges

Sunil Kumar Thamida and Hsueh-Chia Chang
Department of Chemical Engineering, University of Notre Dame, Notre Dame, Indiana 46556

(Received 4 June 2002; accepted 16 September 2002)

We examine a singular electrokinetic flow around a corner or a wedge in micro-channels constructed from dielectric materials whose permittivity is small but finite compared to that of the electrolyte. When the wedge angle is less than 180°, the applied electric field, which is tangential far from the corner, develops a normal surface component that becomes singular at the corner. This normal field leakage causes opposite polarization at the two sides of the wedge and produces a converging singular tangential electrokinetic flow that ejects liquid from the tip. By expanding in cylindrical harmonics, we estimate this ejecting flow as a function of the permittivity ratio, applied electric field, angle of the wedge and the microscopic corner curvature that suppresses the singularity. The ejecting flow entrains tangential flow on the front side of the wedge and produces a vortex on the downstream side. This entrainment offers a long-range attractive hydrodynamic force that complements short-range electrostatic DLVO (Derjaguin–Landau–Verwey–Overbeek) and dielectrophoretic forces to enhance corner deposition and aggregation of colloids and proteins during electrophoresis/electro-osmosis. © *2002 American Institute of Physics.*
[DOI: 10.1063/1.1519530]

PROOF COPY 022212PHF

I. INTRODUCTION

Electrokinetic flow is the mechanism of choice for transporting fluids in future generations of biochips, as it allows easy flow control, metering, and maneuvering.[1] However, one major problem for electrokinetic flow is that proteins tend to precipitate at channel junctions and colloids aggregate at the junction corners. As an example, a submicron latex colloidal suspension is driven electro-osmotically and electrophoretically in water through the micro-channel junction in Fig. 1(a). After about 20 min, colloids aggregate in large amounts around the inner corner of the channel junction as shown in Fig. 1(b). As shown in the figure, the aggregates form a curious and relatively large spiral-like structure that curls downstream and spans nearly half of the 80 μm channel. A small vortex is visible just downstream of the spiral, as shown in Fig. 1(b), when the colloid trajectories are scrutinized with a microscope. The aggregation becomes acute with higher electric fields ($>$30 V/cm) and smaller channels.

Several physical mechanisms can be responsible for the corner aggregation phenomenon. The spiral aggregate exceeds 40 μm in size and is much larger than homogeneous aggregates formed in comparable time by the DLVO (Derjaguin–Landau–Verwey–Overbeek) mechanism.[2] One hence expects a preferential migration of the particles towards the corner that is not present in homogeneous aggregation. As we shall demonstrate in subsequent analysis, both the tangential and normal electric fields are very large at the corner. The latex particles can be polarized by this intense field and migrate by dc dielectrophoresis.[3] This dielectrophoretic migration is driven by electric fields that are highly nonuniform spatially, such as those at the junction corner. The nonuniform field will impart a net force on the bipolar particle despite its opposite charges on the two sides perpendicular to the field line. However, the direction of this dielectrophoretic motion is determined by the difference in the medium and particle dielectric permittivities. For our systems, the dielectric constant of the water medium is 81 and that of the latex particle is 2.5. Hence, the water medium is more polar than the particle and the dielectrophoretic migration should be towards regions with low field intensity. This is clearly opposite of our observation in Fig. 1, where particles migrate towards the high-field corner region. Moreover, dielectrophoretic motion cannot explain the observed vortex. The field nonuniformity will also be shown to exist in only a small neighborhood of the corner whose dimension is much smaller than the aggregate size. Particle polarization occurs and is a key mechanism that holds the aggregate together, but it probably does not contribute to its formation by particle migration towards the corner in this transport-limited aggregation process.

Instead, the large aggregate dimension, the observed vortex, and the aggregate spiral structure that seems to be shaped by the vortex, all suggest that the particle migration towards the corner is driven by hydrodynamic convection. Such a theory is proposed in this article. The small region of high field intensity near the corner is shown to affect the flow in a much larger region by a nonlinear electrokinetic mechanism. We shall demonstrate through theoretical analysis and numerical simulation that this long-range hydrodynamic entrainment mechanism can drive particles to the corner, produce the observed vortex, and allow the formation of a spiral aggregate.

In an electrokinetic flow, fluid is driven by an electric field. Usually, an electric potential drop is applied across the

 © 2002 American Institute of Physics

PROOF COPY 022212PHF

PROOF COPY 022212PHF

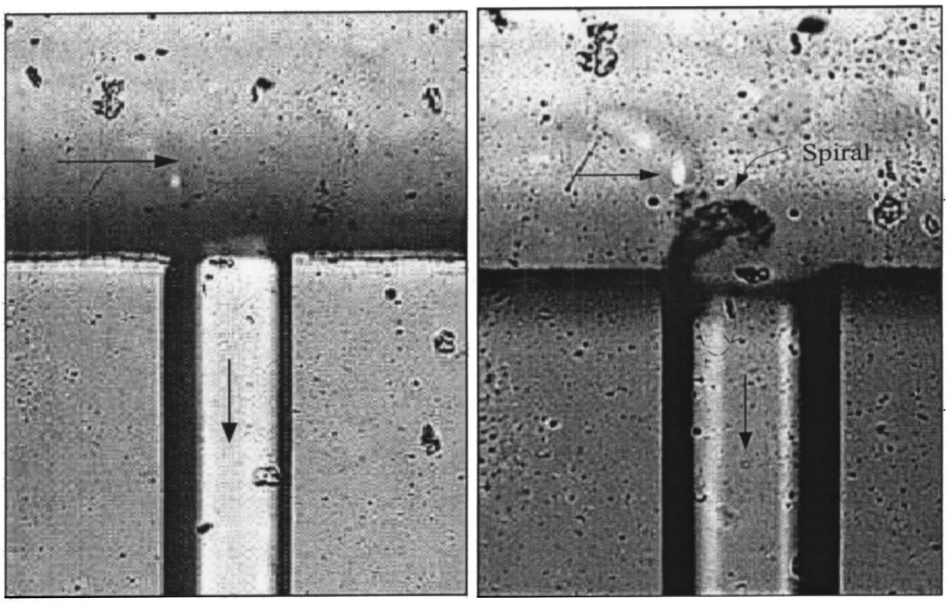

FIG. 1. Experimental snapshot of the micro-channel junction. The narrow channel is 80 μm wide and the latex colloids move towards the narrower channels. The silica channel and the latex colloids are oppositely charged and hence both electrophoretic and electro-osmotic motions are in same direction. (a) During initial stages of electrokinetic flow of submicron colloidal suspension in the direction indicated by the arrow. (b) During later stages showing a spiral colloidal aggregation at the inner corner and a small vortex as sketched schematically.

ends of a channel using electrodes which establishes an electric field parallel to the walls. The micro-channels are made of dielectric materials like silica, polyester, acrylic, etc. Due to surface functional groups, this material creates a charged Debye layer in the electrolyte neighboring it, such that the counter-ions within screen the surface charges. The extent of charge separation in the electrolyte is usually measured by the electric potential across it, the zeta potential ζ, which would be proportional to the surface charge of the wall. For typical dielectric-electrolyte pairs,[2] the potential ζ is in the range of $\pm(25-100)$ mV. Due to the Maxwell body force within the Debye layer, an electric field parallel to the wall drives the bulk fluid at a velocity given by the Smoluchowski slip velocity[4]

$$u_s = -\frac{\epsilon_f \zeta E_t}{\eta}, \tag{1}$$

where ϵ_f is the liquid permittivity, η is its viscosity, and E_t is the tangential field. For dielectric materials with small permittivity compared to the electrolyte, the normal electric field E_n in the wall vanishes and the charge distribution within the Debye layer is independent of the applied field. The polarization in the Debye layer is produced by the field generated by the surface charge. As such, both the zeta potential and the Debye layer thickness are uniform in the entire channel of the same material. Since there is no field leakage and no liquid leakage, this linear electrokinetic slip (1) implies that the velocity field everywhere in the channel is simply

$$\mathbf{u} = -\frac{\epsilon_f \zeta}{\eta}\mathbf{E}, \tag{2}$$

where $\mathbf{E}=-\nabla\phi$ is the electric field. Hence, the electric potential ϕ also becomes the velocity potential and, despite the minuscule Reynolds number in micro-devices ($<10^{-1}$), linear electrokinetic flow behaves like an inviscid potential flow due to the absence of wall shear. The electric field lines coincide with the streamlines in this case for an open channel.[4,5] More interestingly, this potential flow is irrotational and the generation of microscopic vortices in electrokinetic devices for mixing purpose is a major challenge.[6] Yet, Fig. 1(b) indicates that a vortex exists just downstream of the junction. We shall demonstrate that this vortex is generated by a nonuniform zeta potential which is dependent on the applied field. The resulting nonlinear electrokinetic flow produces an ejecting flow from the corner and a back pressure that generates the vortex. This nonlinear electrokinetic phenomenon is a result of field leakage at the corner.

If the dielectric wall has a small dielectric permittivity (mathematically zero) compared to the fluid, then the electric potential around a wedge corner can be solved by decomposing the bulk Ohmic (electro-neutral) region from the wall Debye charged layer and by the usual harmonic expansion.[4] For a wedge angle less than 180°, the tangential field is singular at the corner from classical electrostatic potential theory.[7] However, the normal field remains zero everywhere on the boundary and even the tangential field is smooth away from the boundary. Hence, the coincidence between streamlines and electric field lines still holds away from the corner.

However, biochips are made with dielectrics with a small but finite permittivity. While field leakage is negligible over most of the chip, it is very important at corners because of convexity and the singular tangential field. Using a perturbation analysis, we show that the singular tangential field now leads to a singular normal field that also blows up at the corner. This gives rise to large but opposite polarization on two sides of the corner (see Fig. 2) in addition to the uniform polarization due to surface charges. These normal fields drive two oppositely charged ions to each side. Such polarization produces a destabilizing normal Maxwell stress across a deformable membrane.[8] Here, it produces another instability with a converging electro-osmotic flow towards the corner.

PROOF COPY 022212PHF

PROOF COPY 022212PHF

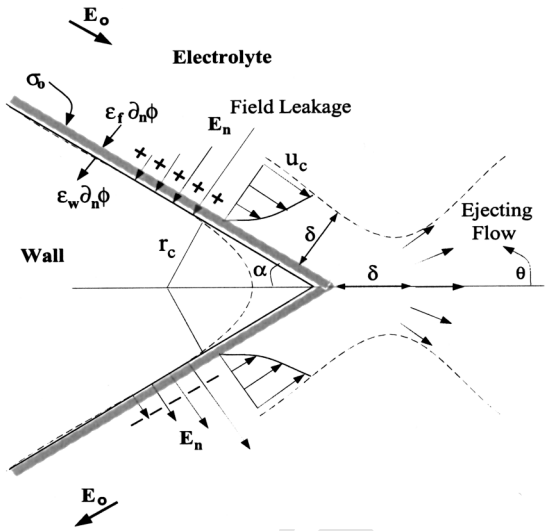

FIG. 2. Schematic diagram showing polarization and the boundary conditions on the electric field of a wall-electrolyte interface around a wedge. A wedge with a finite radius of curvature is also shown.

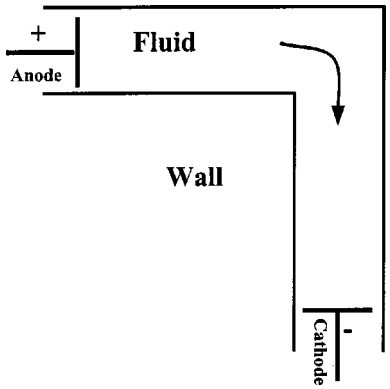

FIG. 3. Schematic diagram of a 90° bend in a micro-channel with electrodes located at far ends.

This instability occurs because the zeta potential near a corner would have opposite contribution from the normal leakage field across the corner, which brings excess ions that overwhelm the original surface charge of the wall. This normal field is singular (infinite) at the corner, localized, and decays to an insignificant amount over a few microns away from the corner. The resulting nonlinear Smoluchowski slip velocity, which is proportional to the product of zeta potential and tangential field, also becomes nonlinear with respect to the applied field, singular at the corner, and changes sign across the corner over a microscopic length. Thus an electrostatic field leakage, though distributed, causes a momentum dipole that produces an ejecting electrokinetic flow from the corner. Although the field penetration length is typically small (<1 μm), the ejection distance (hydrodynamic penetration or entrainment length) is long at tens and hundreds of microns due to the singularity. We estimate the finite strength of this ejecting flow by assigning a finite but microscopic radius of curvature to the corner tip. The ejecting velocity would be directed symmetrically away from the inner corner towards the outer corner and its strength would be a function of the ratio of dielectric permittivities of wall and the fluid, angle of the wedge, the far-away tangential field, zeta potential of the wall, and the radius of curvature of the corner. For atomically sharp corners, the ejecting flow can exceed the bulk electro-kinetic flow.

Due to this strong ejecting flow from the corner, the bulk flow is blocked and vortices develop at the corner. The irrotational feature of linear electrokinetic flow is revoked due to the nonuniform and field-dependent ζ potential at the corner. More precisely, if ζ is nonuniform in (2), the incompressibility condition $\nabla\cdot\mathbf{u}=\mathbf{0}$ no longer produces the Laplace equation for potential flow. We demonstrate vortex formation by obtaining a local solution for the stream function from the biharmonic equation. We also develop a lattice-Boltzmann-method (LBM) code suitable to simulate the outer microfluidic flow in an actual 90° bent channel of finite width. We have implemented a multi-scale approach in which the electrostatics and nonlinear electrokinetic flow near the singular point is dealt analytically while the electrokinetic microhydrodynamics is simulated numerically with a LBM code. Hence, a very high resolution exists within the thin Debye layer for the field-dependent ζ potential and the slip velocity on the channel walls whereas for flow simulation, the lattice node spacing is only of medium resolution—a few microns. The ejecting flow at the corner stipulates a detailed derivation of the corner boundary conditions and lattice spacing. In fact, the long-range corner ejecting flow entrains most of the in-coming flow. With this large hydrodynamic entrainment length of tens to hundreds of microns, colloids and proteins are convected towards the corner and are exposed to the singular normal field. They would then polarize and aggregate due to the classical DLVO mechanism[5] when they are within a submicron neighborhood of the growing aggregate. We propose this long-range hydrodynamic mechanism to be the cause for polarization, alignment, and aggregation of colloids. We obtain the hydrodynamic entrainment fraction through theory and favorably compare it with the multi-scale simulation. Our study then allows us to design channels with minimum hydrodynamic entrainment, protein precipitation and colloid aggregation.

The remaining sections of this article are planned as follows. In Sec. II, we present the governing equations for electrokinetic flow along with the electrostatics in electrolyte and the wall. We propose a model to obtain the normal field leakage and effective nonlinear Smoluchowski slip velocity near a wedge corner. In Sec. III, we obtain a local solution to the vortices and overall flow in the vicinity of the wedge corner. In Sec. IV, we confirm the local results with numerical simulation (LBM) for an electrokinetic flow around a 90° bend.

II. ELECTROSTATICS BY PERTURBATION EXPANSION

Consider the schematic diagram in Fig. 3 depicting a micro-channel with a 90° bend. The electrodes are located at the far ends of each branch. When a potential drop is applied across the electrodes, an electric field would be established in the fluid and also the neighboring wall. Since the fluid is an

PROOF COPY 022212PHF

PROOF COPY 022212PHF

electrolyte, there is a possibility of charge separation and net ionic charge near the channel wall. The electrostatic potential in the electrolyte or the fluid would be governed by the Poisson equation,[4]

$$\nabla^2 \phi = -\frac{\rho}{\epsilon_f}, \tag{3}$$

where ϕ is the electrostatic potential, ρ is the net ionic charge density, and ϵ_f is the dielectric permitivity of the fluid. The potential distribution in the wall, ϕ_w, would also be governed by a similar equation. There is no charge within the solid dielectric material and its potential obeys the Laplace equation,

$$\nabla^2 \phi_w = 0. \tag{4}$$

Note that these equations and the ones to follow are two-dimensional. One spatial variable is along the length and another along the width of the channel. The micro-channels are assumed to have uniform and constant slip velocities at the top and bottom. With its small depth-to-width ratio, the variations in the thin direction can be neglected.[1] The lateral boundary conditions are

$$\phi_w = \phi \quad \text{on side wall,} \tag{5a}$$

$$\epsilon_f \partial_n \phi = \sigma_o + \epsilon_w \partial_n \phi_w \quad \text{on side wall,} \tag{5b}$$

due to continuity of potential and field across the two media. Here, σ_o is the uniform surface charge density on the wall since we use the same functional material along the entire channel.

To solve the above set of equations, one needs to model the ionic concentration distribution in (3) and estimate the cumulative charge density in the fluid,

$$\rho = \sum_i z_i c_i, \tag{6}$$

where c_i is the concentration of ith ionic species and z_i its ionic charge. Ideally, every ionic species should be captured by the full Nernst–Planck convection-diffusion equation with electromigration. However, we will construct specific orthogonal coordinates in a given geometry such that one set of lines is along the direction of ionic flux and the other set of perpendicular lines along which ionic flux is zero. One of these two coordinates correspond to the streamlines. There is hence no convection in the other coordinate orthogonal to the streamlines. The only ion flux mechanisms along them are diffusion and electromigration. Moreover, since the wall is a streamline, the latter orthogonal coordinates must terminate at the wall. Since there is no ion flux into the wall, electromigration must then cancel diffusion exactly everywhere along this set of no-flux lines. Thermodynamic equilibrium must exist along these lines and everywhere the lines are defined on a plane. A simple integration of the convectionless Nernst–Planck equation along these lines then yields the equilibrium Boltzmann distribution,[4]

$$c_i = c_{i,o} \exp\left(\frac{-z_i \mathrm{F} \psi}{RT}\right), \tag{7}$$

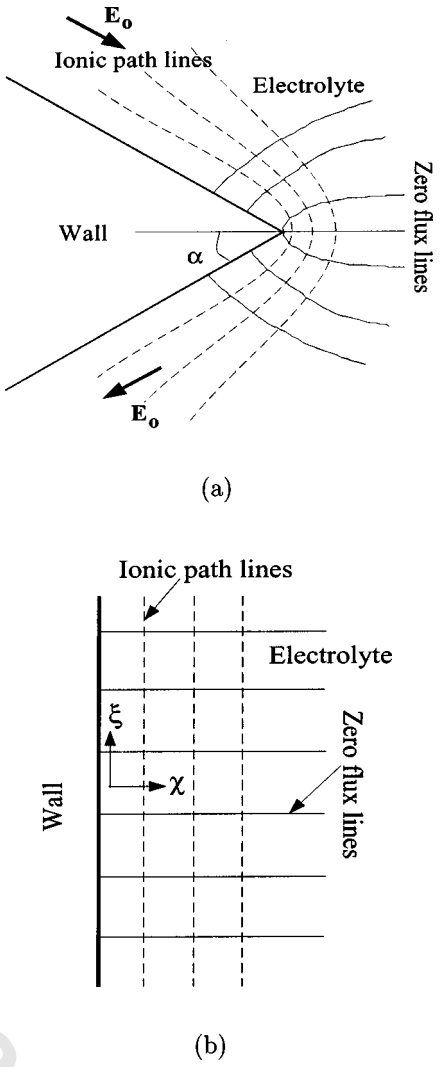

FIG. 4. Schematic diagram showing the ionic path lines and zero flux lines around a wedge in (a) actual geometry and (b) transformed orthogonal coordinates.

where $c_{i,o}$ is the concentration of ith ionic species in the bulk, ψ is the over-potential relative to the potential in the bulk, F is the Faraday constant, R is the gas constant, and T is the temperature of the fluid. As described earlier regarding the orthogonal coordinates, ψ would be the potential along those set of orthogonal lines that emanate from the impermeable wall and along which there is no ionic flux. These lines would be perpendicular to the wall in straight channels. The thickness of the Debye layer is simply the characteristic length along these lines over which ψ decays to the zero reference value in the bulk. For the case of a wedge, the thickness is measured along the no-flux coordinate. This no-flux coordinate is multi-valued at the cusp, as shown in Fig. 4(a). The equilibrium Boltzmann distribution (7) hence becomes undefined exactly at the cusp. However, we shall smooth the cusp with an effective radius of curvature in our theory and the singularity exactly at wedge corner is not significant. Since the leading-order Ohmic field and the wall field are determined by the Laplace equation, we shall make extensive use of the conformal map of the cylindrical (r,θ) coordinates of the wedge to rectilinear (χ,ξ) coordinates

PROOF COPY 022212PHF

PROOF COPY 022212PHF

along a flat plane as shown in Fig. 4(b). Away from the corner, the latter coordinates will also be shown to be the desired orthogonal streamlines and no-flux lines for the Boltzmann distribution and the Debye layer thickness.

Since the normal field in the Debye layer far exceeds the applied tangential field, classical electrokinetic theory[4] decomposes the fluid potential ϕ into the Ohmic potential Φ, representing the tangential field for the neutral bulk that sees an insulated wall, and an over potential ψ, representing the normal field in the polarized Debye layer. Moreover, the over potential ψ obeys the Poisson equation with a wall flux specified by the surface charge through (5b). [In the classical case, the wall is insulated and ϵ_w is zero exactly in (5b).]

Since $\partial_n\psi \gg \partial_t\Phi$, this decomposition allows an expansion of the quadratic nonlinear Maxwell term in the momentum equation such that it becomes linear in the tangential field $\partial_t\Phi$. This expansion leads to the slip velocity (1) directly. Moreover, the decomposition allows a one-dimensional resolution of ψ and the momentum equation due to the corresponding length-scale separation (between the Debye layer and the channel dimensions) that accompanies the separation in the field strengths. Finally, the harmonic, Ohmic potential obeys the Laplace equation with insulated walls and is hence easy to resolve with mathematical techniques like conformal maps.

We shall also employ the same convenient decomposition of the fluid potential ϕ into an Ohmic component Φ and an over potential component ψ. At the wall polarized layer, $\partial_n\psi \gg \partial_n\Phi$ as in classical theories. This large field $\partial_n\psi$ is attributed to the surface charge σ_o in (5b). The new wall leakage term $\epsilon_w\partial_n\phi_w$ is negligible away from the corner but must be comparable to σ_o near it to reverse the polarization as shown in Fig. 2. We hence associate the wall leakage $\epsilon_w\partial_n\phi_w$ in (5b) to the dominant $\epsilon_f\partial_n\psi$ and σ_o terms on the fluid side to produce a new boundary condition. The remaining term $\epsilon_f\partial_n\Phi$ for the wall Ohmic field on the fluid side is much smaller than these three terms. Hence, to leading order, the fluid Ohmic potential obeys a no-flux condition at the wall. We note that the wall field leakage term $\epsilon_w\partial_n\phi_w$ has opposite signs across the corner while σ_o has always the same sign. Hence, the wall field on the liquid side $\epsilon_f\partial_n\psi$ can have opposite signs across the corner—the polarization and slip velocity can change sign across the corner. The sign change is in fact necessary for back flow and vortex formation. Our theory will produce a new slip velocity that reduces to the classical version (1) when the field leakage is absent. Decomposing the fluid potential ϕ as stated,

$$\phi = \Phi + \psi, \tag{8}$$

where Φ is the Ohmic potential governing the tangential transport of neutral electrolyte and ψ is the over potential across the polarized layer near the wall due to field leakage at the corner. As such, the linear boundary condition (5b) without the surface charge term is decomposed into a no-flux condition for Φ and a gradient condition for ψ that is determined by the surface charge σ_o and the wall field $\epsilon_w\partial_n\phi_w$. We solve for Φ and ψ iteratively by also employing the Boltzmann distribution (7) and using boundary conditions (5) alternatively in the iteration.

The leading-order Ohmic potential in the fluid is hence governed by the following equations in the cylindrical coordinates centered around the wedge corner as in Fig. 4(a),

$$\nabla^2\Phi = 0, \tag{9a}$$

$$\partial_n\Phi = 0 \quad \text{at} \quad \theta = \pm(\pi - \alpha). \tag{9b}$$

The large fluid electric field at the wall, as governed by (5b), is assigned to that of the over potential ψ. The solution to the Ohmic potential of (9a) in the physical coordinates is an eigenfunction expansion in the cylindrical harmonics of the Laplace equation that satisfy the boundary conditions (9b),

$$\Phi = Ar^{\lambda}\sin\lambda\theta, \tag{10a}$$

where

$$\lambda = \frac{(2n+1)\pi}{2(\pi-\alpha)}, \quad n = 0, \ \pm 1, \ \pm 2, \ldots . \tag{10b}$$

If the wedge were a corner in the bent channel, then the field far from the corner should be a constant in either of the channel branches. Only one eigenfunction corresponding to $n=0$ would not blow up far away and be zero at the line of symmetry at $\theta=0$. Hence for every wedge of certain angle α there is only one possible eigenfunction with eigenvalue $\lambda=\pi/2(\pi-\alpha)$. The constant A would then be obtained from matching with the outer solution. Though the actual value of A is case dependent, it is clear that it scales linearly with the applied field E_0. Let $A=A^*E_oW$ with A^* a dimensionless constant, E_o the constant electric field in the channel far from the corner, and W the width of the channel. The dimensionless space variable in (10a) is $r=\hat{r}/W$ where $\hat{r}$ is the actual dimensional radial position. Since the far-way field is constant at E_o, it is chosen as the appropriate electric field scaling. An appropriate length scale is the width of the channel W since the effect of a wedge in a bent channel is assumed to persist only over a distance of the width of the channel, which is a reasonable one to assume because beyond a distance equal to width from the corner, both the walls are parallel and the field would be nearly a constant. From numerical solution in bent channels, it will be shown that $A \approx (1.0-1.2)E_oW$, for all angles of the wedge $0<\alpha<\pi/2$.

We next determine the wall potential ϕ_w governed by the Laplace equation (4). Although the normal field strength of the over potential $\partial_n\psi$ is much larger than $\partial_t\Phi$ or $\partial_n\Phi$ of the Ohmic field, the actual potential drop across the polarized layer is small compared to the wall Ohmic potential drop across the corner due to leakage. For Debye layers, the zeta potential is the potential drop and is of the order of 25–200 mV. While the over potential with field leakage is higher on one side, we do not expect it to exceed 200 mV, which is far smaller than the drop in the wall Ohmic potential across the corner when leakage exists. We hence neglect ψ in (5a) and use the Ohmic potential continuity condition

$$\phi_w = \Phi \quad \text{at} \quad \theta = \pm(\pi - \alpha), \tag{11}$$

The solution to the wall potential distribution can then be obtained from (4) with boundary condition (11) as

PROOF COPY 022212PHF

PROOF COPY 022212PHF

$$\phi_w = Ar^{\lambda}\frac{\sin\lambda(\pi-\theta)}{\sin\lambda\alpha}. \tag{12}$$

The normal field leakage part of E_n in the adjacent electrolyte at the wall is then

$$\frac{\epsilon_w}{\epsilon_f}\partial_n\phi_w = \mp\frac{\epsilon_w}{\epsilon_f}\frac{A}{W}\lambda\cot\lambda\alpha\, r^{-(1-\lambda)} \quad \text{at} \quad \theta=\pm(\pi-\alpha). \tag{13}$$

It can be seen from the schematic in Fig. 2 that the normal field changes sign in the region near the corner. It is because the field leakage enters from the fluid at $\theta=(\pi-\alpha)$ and reenters the fluid at $\theta=-(\pi-\alpha)$. Without surface charge, this field leakage would establish Boltzmann distributions of oppositely charged ions and create oppositely polarized surfaces on the opposite edges of the wedge, rendering the wedge corner bipolar. We have shown in an earlier work that electrokinetic flow past a large bipolar particle can produce back-flow and vortices.[6] Here, back flow and vortices develop because the zeta potential changes sign across the corner and the resulting Smoluchowski slip velocity converges towards the corner. The tangential slip velocity hence decreases and changes sign around a corner and continuity stipulates that a back pressure must appear to eject the flow, as sketched in Fig. 2. This back pressure also generates the downstream vortex. However, the coefficient A will be determined through matched asymptotics with a constant field applied far from the wedge. This far-field behavior depends on the channel geometry and will be resolved numerically in a later section with a finite channel width. The effect of surface charge, ignored in the above argument, will also be included.

Although the Ohmic field and wall potentials are solved in the original cylindrical coordinates of the wedge, we shall solve for ψ in the transformed coordinates (χ,ξ) of Fig. 4(b). These coordinates are defined by the conformal map that maps the wedge into a plane. They are both harmonic functions that satisfy the Laplace equation $\nabla^2\xi=\nabla^2\chi=0$. Insofar as the Ohmic fluid potential Φ is a harmonic function for the wedge geometry, the ξ coordinate simply corresponds to a dimensionless version of Φ. The constant ξ contours are isopotential contours. The orthogonal constant χ contours correspond to the streamlines of linear electrokinetic flow with an insulated wedge. Hence, the orthogonal coordinates χ are the desired no-flux lines along which the Boltzmann distribution (7) can be derived and the Debye layer thickness can be defined. The Boltzmann distribution hence holds everywhere the χ coordinates are defined. Near the corner, wall leakage would mean that χ coordinates are no longer the no-flux lines but are good approximations of them near the wall. At precisely the corner point, however, no-flux lines cannot be defined at all. Hence, the Boltzmann distribution (7) is valid everywhere except at the corner and a small sector beyond it.

We can then use (7) to determine the net charge density $\rho=\Sigma_i z_i c_i$ everywhere except the point on the corner. Since the Ohmic potential Φ is a harmonic function, (3) then yields

$$\nabla^2\psi = -\frac{\Sigma_i z_i c_{i,o}\exp(-z_i F\psi/RT)}{\epsilon_f}. \tag{14a}$$

The boundary condition (5b) on the normal electric field now produces a condition for the over-potential ψ on the liquid side,

$$\partial_n\psi = E_n = \frac{\sigma_o}{\epsilon_f} + \frac{\epsilon_w}{\epsilon_f}\partial_n\phi_w \quad \text{at} \quad \theta=\pm(\pi-\alpha), \tag{14b}$$

where E_n represents the normal electric field near the wall on the fluid side and includes both surface charge and field leakage contributions. Another boundary condition is that $\psi\to 0$ far from the wall. If $\psi<RT/F$ throughout, then we can further invoke the Debye–Huckel approximation[2] on (14a) by expanding in $(z_i F\psi/RT)$ and transforming the Poisson–Boltzmann equation to a linear partial differential equation,

$$\frac{1}{W^2}\nabla^2_{r,\theta}\psi = \frac{\psi}{\delta^2}, \tag{15}$$

where $\delta=(\Sigma_i c_{i,o}F^2 z_i^2/\epsilon_f RT)^{-1/2}$ is the Debye length and use has been made of the electric neutrality condition at large χ, that is $\Sigma_i z_i c_i = 0$.

We now transform this Poisson equation by the conformal map of the wedge to a plane in Fig. 4(b). The ξ variable is the Ohmic potential function $\Phi(r,\theta)$ in its dimensionless form and χ corresponds to the field lines. We get from (10)

$$\chi = A^* r^{\lambda}\cos\lambda\theta, \tag{16a}$$

$$\xi = A^* r^{\lambda}\sin\lambda\theta, \tag{16b}$$

where $\chi=\hat{\chi}/W$ and $\xi=\hat{\xi}/W$ with χ and ξ being the dimensionless coordinates. Transforming (15) from (r,θ) coordinates to (χ,ξ) coordinates gives

$$\frac{|\nabla\xi|^2}{W^2}\nabla^2_{\chi,\xi}\psi = \frac{\psi}{\delta^2}, \tag{17}$$

where $\nabla^2_{\chi,\xi}=\partial^2/\partial\chi^2+\partial^2/\partial\xi^2$ is the Laplace operator in rectilinear coordinates. Since ξ is same as the nondimensional potential function, the nonlinear coefficient $|\nabla\xi|^2=\|\mathbf{E}\|^2/E_o^2$ where $\mathbf{E}=-\nabla\Phi$ is the local Ohmic electric field. Since this Ohmic field does not leak into the wall, $\|\mathbf{E}\|=|\partial_t\Phi|=|E_t|$ at the wall. The field E_o is the far field used to scale Φ. In the appropriate variables of (χ,ξ), it can be shown that $|\nabla\xi|^2=\lambda^2(\xi^2+\chi^2)^{-(1-\lambda)/\lambda}$. Since the Debye layer is very close to the wall, that is $\theta\to\pm(\pi-\alpha)$, it would imply that $\chi\to 0$ and $\partial/\partial\xi\ll\partial/\partial\chi$ which upon substituting in (17) gives an ordinary differential equation in χ as

$$\frac{d^2\psi}{d\hat{\chi}^2} = \frac{\psi}{(E_t/E_o)^2\delta^2}, \tag{18}$$

where $E_t=\lambda\xi^{-(1-\lambda)/\lambda}$ is the tangential field at the wall which is only a function of ξ and is independent of χ. Note that $\hat{\chi}$ is the dimensional form of χ, that is, $\hat{\chi}=W\chi$ where W is the width of the channel. The boundary conditions in (14) on ψ in the transformed variables are

$$-\frac{\partial\psi}{\partial\hat{\chi}} = \frac{E_n}{(E_t/E_o)} \quad \text{at} \quad \hat{\chi}=0 \tag{19a}$$

PROOF COPY 022212PHF

PROOF COPY 022212PHF

$$\psi = 0 \quad \text{at } \hat{\chi} \to \infty. \tag{19b}$$

Integration of (18) with (19a) and (19b) then yields the field-dependent ζ, the value of ψ at $\hat{\chi}=0$,

$$\zeta = E_n \delta. \tag{20}$$

Note that unlike for a plane wall, the Debye layer thickness from (18) near a sharp corner is larger by a factor of E_t/E_o. But, the normal field in (19a) is reduced by the same factor E_t/E_o. Hence these opposing contributions cancel each other and the formula for zeta potential given in (20) remains the same as for a plane wall which is equal to the product of the normal field at the wall and Debye layer thickness. Since $E_t = -\partial_t \Phi$ is singular at the wedge, (18) becomes invalid at the corner as shown in Fig. 4(a). However, we expect (20) to be valid away from some neighborhood of the corner.

If E_n is too large or $\zeta \gg RT/F$, then the above approximation would overshoot the actual value that would be obtained by solving (14a) and (14b) exactly. Then, we would have to use either Gouy-Chapman theory for symmetrical electrolytes or Grahame's analysis for asymmetrical electrolytes.[2] Note from (14b) that the normal field at the wall E_n and the ζ potential in (20) would consist of two parts, one is due to the field of surface charge (σ_o/ϵ_f) and the second is due to field $(\epsilon_w/\epsilon_f)\partial_n \phi_w$ in the wall neighboring the fluid. With singular field leakage, the second contribution becomes dominant in the vicinity of the corner.

We can now estimate the zeta potential from (20) by substituting (13) and (14b) to obtain the natural and induced ζ potentials,

$$\zeta = \zeta_o + \zeta_1, \tag{21a}$$

$$\zeta_o = \left(\frac{\sigma_o}{\epsilon_f}\right)\delta, \tag{21b}$$

$$\zeta_1 = \mp \frac{\epsilon_w}{\epsilon_f}\delta \frac{A}{W}\lambda \cot \lambda\alpha\, r^{-(1-\lambda)} \quad \text{at } \theta = \pm(\pi - \alpha_f). \tag{21c}$$

The linear and nonlinear parts of Smoluchowski slip velocity can then be estimated by substituting (21) in (1),

$$u_s = u_{s,o} + u_{s,1}, \tag{22a}$$

$$\left(\frac{\eta}{\epsilon_f}\right)u_{s,o} = -\zeta_o E_t = -\zeta_o \frac{A}{W}\lambda r^{-(1-\lambda)}, \tag{22b}$$

$$\left(\frac{\eta}{\epsilon_f}\right)u_{s,1} = -\zeta_1 E_t = \pm \frac{\epsilon_w}{\epsilon_f}\delta \cot \lambda\alpha E_t^2 = \pm \frac{\epsilon_w}{\epsilon_f}\delta \frac{A^2}{W^2}\lambda^2 \cot \lambda\alpha\, r^{-2(1-\lambda)} \quad \text{at } \theta = \pm(\pi - \alpha), \tag{22c}$$

where $u_{s,o}$ is the linear slip velocity in the absence of field leakage effects and $u_{s,1}$ is the additional nonlinear slip velocity due to corner field leakage. The linearity and nonlinearity refer to the scalings with respect to the local tangential field E_t which is linear for $u_{s,o}$ while quadratic for $u_{s,1}$. The nonlinear slip exists only near the corner where it actually dominates the linear slip. The nonlinear slip velocity has opposite signs on either sides of the wedge which implies that it is directed towards the corner on either sides.

Moreover, the nonlinear slip occurs only if $\lambda < 1$, that is for wedge angles less than π or $\alpha < \pi/2$ from (10b). Hence there would be field leakage at the inner corner of a bent channel of Fig. 3. However, for the outer corner, with angle $3\pi/2$ greater than π, the eigenvalue λ will be greater than 1 and there would not be any field leakage, polarization, or vortex formation. This explains why protein and colloid aggregates are never found at the outside corner. Moreover, the induced ζ_1 changes sign across the wedge corner.

III. LOCAL HYDRODYNAMICS

When we solve for the hydrodynamic flow, the stream function can also be split into two parts, one for linear and one for nonlinear electrokinetics,

$$\Psi = \Psi_o + \Psi_1. \tag{23}$$

The first one would be due to the linear slip velocity $u_{s,o}$ caused by the uniform surface charge with a constant zeta potential, ζ_o. The second part is due to nonlinear slip velocity $u_{s,1}$ caused by the nonuniform zeta potential ζ_1 due to field leakage. The linear electrokinetic flow biharmonic equation with uniform slip is

$$\nabla^4 \Psi_o = 0, \tag{24a}$$

$$u_n = -\partial_t \Psi_o = 0 \quad \text{at } \theta = \pm(\pi - \alpha), \tag{24b}$$

$$u_t = \partial_n \Psi_o = u_{s,o} \quad \text{at } \theta = \pm(\pi - \alpha). \tag{24c}$$

With linear slip, it corresponds to potential flow. Hence, of all the cylindrical harmonics of the biharmonic equation, only one Laplace harmonic survives—the same one as the electro-static harmonic (10a) with $\lambda = \pi/2(\pi - \alpha)$,

$$\Psi_0 = C r^{\lambda} \cos \lambda\theta. \tag{25}$$

The streamlines of this linear electrokinetic flow are hence exactly identical to the electric field lines, as shown in Fig. 5(a). The magnitude of the coefficient C would be proportional to the bulk flow rate $u_o W$ as $C = A^* u_o W$, where A^* is the same constant that would appear in the potential function of (10a).

The nonlinear electrokinetic flow stream function Ψ_1 must be governed by a biharmonic equation as in (24a) and have zero normal flux of fluid at the walls of the wedge,

$$\partial_t \Psi_1 = 0 \quad \text{at } \theta = \pm(\pi - \alpha), \tag{26}$$

and yield opposite tangential velocities on the two sides of the wedge, as shown in Fig. 5(b). Hence, the only permissible harmonics of the biharmonic equation are

$$\Psi_1 = D r^{\beta} \sin \beta\theta \tag{27}$$

with $\beta = n\pi/(\pi - \alpha)$, $n = \pm 1, \pm 2, \ldots$. Since there is an outer wall, the momentum of the ejected flow should decay due to back pressure and it stipulates that $\Psi_1 \to 0$ as $r \to \infty$. Retaining the dominant singular harmonic that decays the slowest, we obtain $n = -1$ and $\beta = -\pi/(\pi - \alpha)$. The value of this exponent β is exactly negative of twice of the exponent λ for

PROOF COPY 022212PHF

PROOF COPY 022212PHF

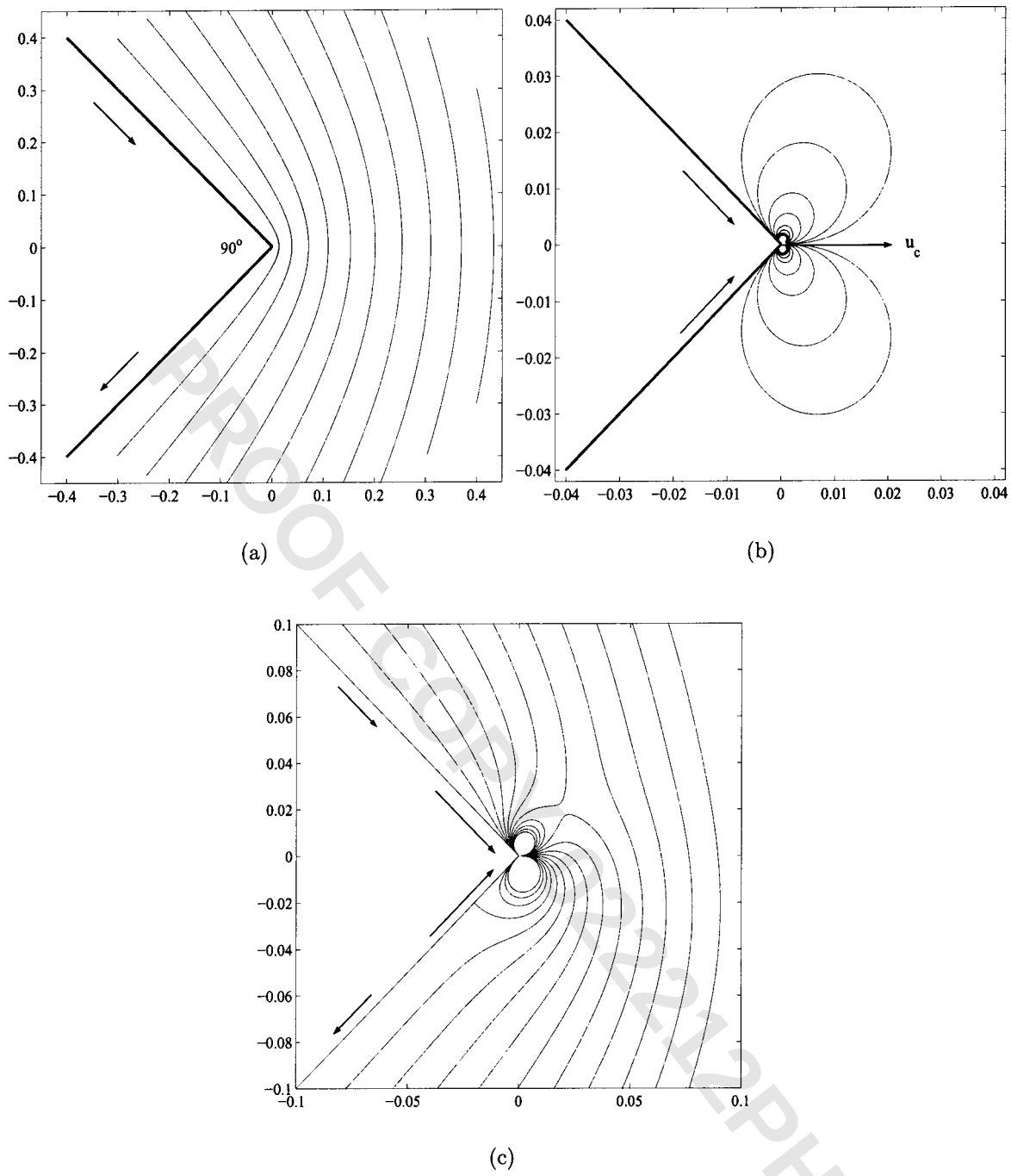

FIG. 5. Streamlines of electrokinetic flow around a wedge. (a) Linear electrokinetic flow Ψ_o for a perfectly insulating wall. Equation (25) with $C=1$. (b) Vortex stream function Ψ_1 due to field leakage effect. Equation (27) with $D=0.0004$. (c) Overall stream function $\Psi=\Psi_o+\Psi_1$.

the electrokinetic stream function in (10a). However, the exponent β is incompatible with that of the nonlinear slip (22c) for any positive wedge angle α, since

$$\beta-1=-2\lambda-1\neq 2(\lambda-1). \tag{28}$$

In fact, the exponent of the nonlinear slip velocity is incompatible with any of the harmonics in (27) for any wedge angle $\alpha<\pi/2$. Unlike its linear electrokinetic flow counterpart, the nonlinear creeping electrokinetic flow at a wedge is strictly ill-posed. The difficulty may arise from the absence of a normal and the inability to define a slip direction at the tip. However, real wedges are not infinitely sharp but rather have a finite radius of curvature, as seen in Fig. 2. This regularized problem is well-posed and the incompatible harmonics of (27) can still be used to approximate its solution. A finite ejecting flow of strength $u_c\delta$ now exists for the smoothed cusp as shown in Fig. 2 and it is taken to be the total flow within the Debye layer on either sides of the wedge converging towards the tip. If the tip is rounded off to a radius r_c, then u_c can be evaluated from $u_{s,1}$ of (22c) at a distance $r_*=r_c\cot\alpha$ from the tip along the wedge wall:

$$\left(\frac{\eta}{\epsilon_f}\right)u_c=\frac{\epsilon_w}{\epsilon_f}\,\delta\frac{A^2}{W^2}\lambda^2\cot\lambda\alpha\left(\frac{r_*}{W}\right)^{-2(1-\lambda)}. \tag{29a}$$

PROOF COPY 022212PHF

PROOF COPY 022212PHF

If we invoke the matched asymptotic result, $A=A^*E_oW$, where A^* has to be determined later, a more explicit estimate of u_c can be obtained as

$$u_c=\left(\frac{\epsilon_f}{\eta}\right)\frac{\epsilon_w}{\epsilon_f}\,\delta E_o^2 A^{*2}\lambda^2\cot\lambda\alpha\left(\frac{r_*}{W}\right)^{-2(1-\lambda)}. \tag{29b}$$

The ejecting velocity can be compared to the far-field electrokinetic flow velocity u_o given by (1),

$$\frac{u_c}{u_o}=\left(\frac{\epsilon_w}{\epsilon_f}\right)\left(\frac{E_o\delta}{\zeta_o}\right)A^{*2}\lambda^2\cot\lambda\alpha\left(\frac{r_*}{W}\right)^{-2(1-\lambda)} \tag{29c}$$

For a 90° bend ($\alpha=\pi/4$, $\lambda=\frac{2}{3}$), the ejecting velocity becomes comparable to u_o for $(r_*/W)\approx 10^{-4}$ for a typical values of $(\epsilon_w/\epsilon_f)\approx\frac{1}{20}$, $\delta\approx 50$ nm, $\zeta_o\approx 50$ mV, and $E_o\approx 100$ V/cm. For a mm-dimension channel, this is reached at r_c of roughly 100 nm, a reasonable roughness scale for silica channels fabricated by plasma etching. Due to the $\cot\alpha$ scaling, this critical ejecting velocity becomes even more severe for sharp edges. As shown in Fig. 2, it produces an ejecting flow of strength $u_c\delta$ at a radius roughly equal to that of Debye layer thickness δ. This gives an estimate of D that is the strength of the circulating vortices and we get Ψ_1 in (27) as

$$\Psi_1=\left(\frac{u_c\delta}{2}\right)\left(\frac{r}{\delta}\right)^{-2\lambda}\sin 2\lambda\theta. \tag{30}$$

However, we do not expect the flow near the wedge to be dominated by only one Stokes harmonic, especially one with an incompatible exponent from the nonlinear slip. The incompatibility gives rise to an error that grows towards the corner. Rather, (30) should only be valid sufficiently far from the wedge. In fact, we shall show from our subsequent simulation that, with a sufficiently sharp wedge, the flow near the wedge is a radial potential flow.

Nevertheless, the existence of vortices and hydrodynamic entrainment can be estimated from Ψ_1. The streamlines of linear electrokinetic flow Ψ_0, nonlinear electrokinetic flow Ψ_1, and the combined flow $\Psi_0+\Psi_1$ are shown in Figs. 5(a)–5(c). It can be seen from Fig. 5(c) that the streamlines are drawn towards the corner on the front side of the wedge. All the streamlines approaching the corner are bent inwards and make a half circulation before passing on to other side of the wedge. This hydrodynamic entrainment is due to the ejecting momentum at the corner. The amount of flow that is entrained can be estimated from the value of the overall stream function near the wedge. Near the corner, the circulatory flow due to Ψ_1 would be the dominating one. It can be estimated as the maximum value of Ψ_1 or total ejecting flow from (30) in the region of singularity, that is, $r\to\delta$ and $0<\theta<(\pi-\alpha)/2$. If Ψ_e is the fraction of the flow entrained, then

$$\Psi_e=\frac{u_c\delta}{2}. \tag{31}$$

Hence the entrainment efficiency Ψ_e^* that is the ratio of Ψ_e to the total flow u_oW scales as

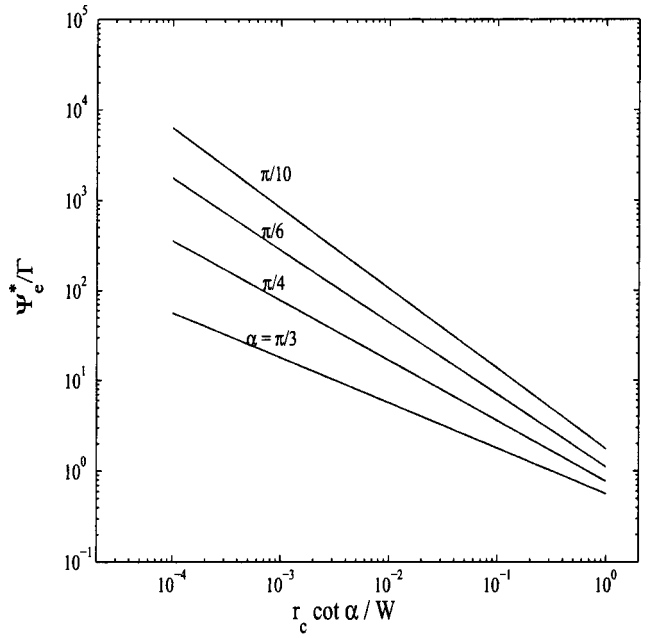

FIG. 6. The entrainment stream function Ψ_e^* scales as a power-law with respect to r_c and increases with decreasing wedge angle, α. Here Γ is the coefficient in (32), $\Gamma=(\epsilon_w/\epsilon_f)(E_o\delta/\zeta_0)(\delta/W)A^{*2}(\lambda^2/2)\cot\lambda\alpha$.

$$\Psi_e^*=\left(\frac{\epsilon_w}{\epsilon_f}\right)\left(\frac{E_o\delta}{\zeta_0}\right)\left(\frac{\delta}{W}\right)A^{*2}\frac{\lambda^2}{2}\cot\lambda\alpha\left(\frac{r_c\cot\alpha}{W}\right)^{-2(1-\lambda)}. \tag{32}$$

The channel width is W and a pure electrokinetic flow with a flat velocity profile u_o described by the Smoluchowski slip (1) has been assumed far from the corner. We will demonstrate from subsequent matched asymptotic result for the electric field in finite-width channels that $A^*\approx 1$ for all wedge angles less than π. The entrainment efficiency, Ψ_e^*, has complex scalings with respect to α and a power-law scaling with respect to r_c. Nevertheless, it increases with decreasing α and r_c, as seen in Fig. 6. If the wedge were a corner in a bent channel with a known flow rate (wall stream function), then it can be predicted that the entire flow could be entrained if Ψ_e is equal to the wall stream function. This critical condition depends on the angle of the wedge, radius of curvature or sharpness, dielectric constant of the wall, the mean electric field, Debye layer thickness, width of the channel, and the mean zeta potential.

On the front side of the wedge, both main flow stream function Ψ_o and the ejecting flow stream function Ψ_1 are positive whereas on the back side of the wedge, Ψ_o is positive while Ψ_1 is negative. The resultant overall flow would have a back-flow or a vortex in the back side wherever the overall stream function is negative. The size of this vortex is insignificant for smaller strengths of the ejecting velocity, but it increases gradually as the ejecting velocity u_c increases. A vortex also appears at the upstream side but tends to be much weaker. The current analysis is a local one near the corner. Only dominant harmonics have been retained and the flow near the wedge can be very different from (30). The outer flow can also distort the vortices in Fig. 5(c). However, the back vortex and the entrainment condition (31) would be

PROOF COPY 022212PHF

PROOF COPY 022212PHF

verified for an actual 90° bend with numerical simulation (LBM) in the following section, where we remove the nonlinear slip and use the estimated ejecting velocity u_c of (29c) in an appropriate manner to capture the ejecting flow due to field leakage.

IV. NUMERICAL FLOW SIMULATION

The nonlinear ejecting flow due to field leakage is localized to the inner corner and we use (29b) or (29c) to model its effects. The simulation is done on the remaining domains with a linear slip where field leakage is absent. We hence impose (1) or (22b) with $\zeta=\zeta_0$ of the natural ζ potential. It is necessary to solve the Ohmic electric field without leakage in a bent channel of Fig. 3 with wedge angle α and unit width. A numerical Laplace solver[9] is used to solve Eq. (9a) with no-flux boundary condition (9b) on the walls and the far away electric field is set to unity. The magnitude of the tangential electric field along the inner wall and the outer wall of a 90° channel are plotted in Fig. 7(a). As expected, the field near inner corner bears a singularity and decreases monotonically to its far field value of unity over a distance equal to the width of the channel. For the outer wall, field is zero at the corner and increases monotonically to its far field value of unity over a distance equal to the width of the channel. The outer corner does not bear a singularity as the singularity occurs only for wedge angles (the angle on the wall side) less than 180°. The Ohmic tangential field from (10a) is $E_t=A^*E_o\lambda r^{-(1-\lambda)}$ on the inner wall near the wedge where E_t must scale linearly with respect to the far-away field E_o being set to unity. The magnitude of the coefficient A^* is obtained from its asymptotic value as $r\to 0$ for various wedge angles and it is plotted in Fig. 7(b). It is clear that the coefficient is nearly a constant of order unity $A^*\approx 1$. We have even simulated walls with a finite but small dielectric permittivity. The tangential field away from the corner does not vary much from the solution plotted in Fig. 7(a) for perfectly insulating walls. The field profile near the corner shifts downwards as the dielectric constant of the wall increases. We can use $A^*=1$ in (32) to estimate the capture efficiency of an arbitrary wedge.

To verify the accuracy of (30) and (31), we have developed a lattice Boltzmann method (LBM) code for simulating the flow. It is a mesoscopic simulation technique for fluid flows and other transport phenomena.[10] It incorporates the features of density probability distribution, single relaxation time constant, discretized spatial lattice, discrete particle velocities. We refer to the literature for the simulation technique.[11] For our purpose, we choose the one that corresponds to an incompressible fluid and that recovers the solution to Navier–Stokes equation. As shown in the schematic Fig. 8, for a 90° bend channel, a square lattice is used with nine velocity directions resolved at each lattice node.[11] In total, there are 100 nodes along the width of the channel and 400 nodes along the length.

Because the ejecting velocity (29b) is obtained via a flow balance within the Debye layer, the slip and ejecting boundary conditions imposed on the wall nodes of the LBM code must be done with care. Linear and nonlinear electro-

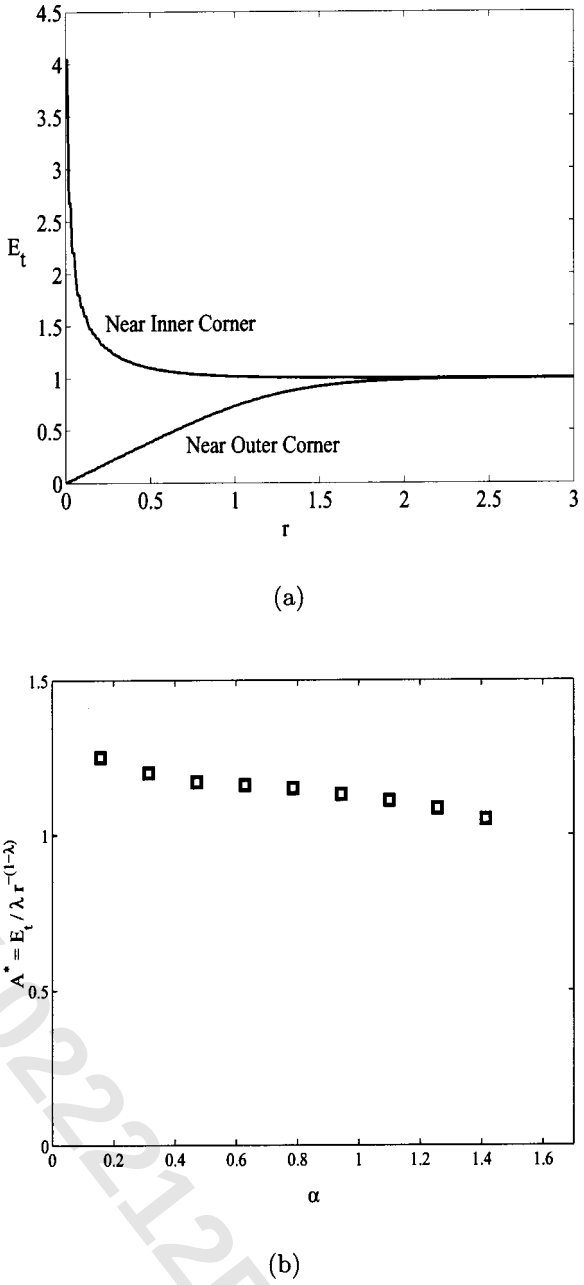

FIG. 7. (a) Electric field variation along the length of a 90° channel at inner corner and outer corner. (b) The magnitude of the harmonic coefficient A^* obtained from its asymptotic value at $r\to 0$ for various wedge angles α in radians.

kinetic tangential velocities approach constant asymptotic values away from the wall, giving rise to effective universal slip expressions like the linear Smoluchowski slip (1) or (22b) and our nonlinear version (22c). This is because the bulk is neutral and the Maxwell stress vanishes away from the polarized layer. The universality means that the slip velocity can be applied anywhere near or on the boundary, as far as the outer flow is concerned. Such asymptotic behavior does not exist for normal ejection velocity from the corner. Due to either radial mass flux considerations or momentum loss, it decays monotonically from the corner. As such a universal effective boundary condition does not exist for the normal ejection velocity, its value depends on where this

PROOF COPY 022212PHF

PROOF COPY 022212PHF

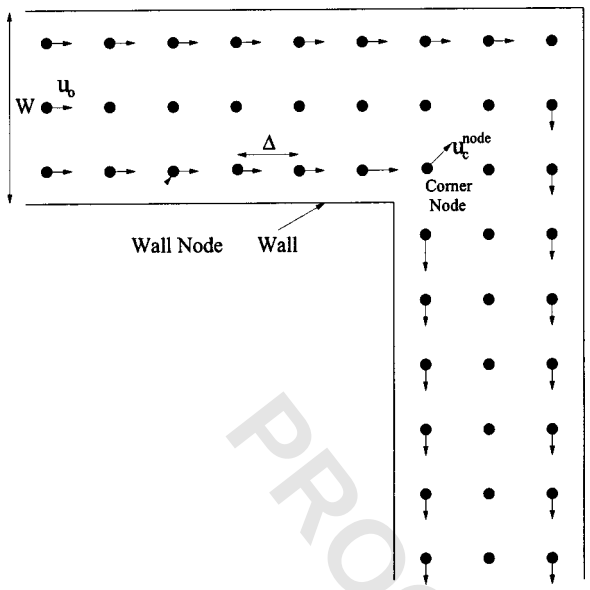

FIG. 8. Schematic diagram of slip boundary condition for LBM simulation of electrokinetic flow in a micro-channel with a 90° bend. The channel width W is scaled to unity.

boundary condition is imposed for the outer flow and this location cannot be exactly at the wall. It hence becomes a lattice-size-dependent effective normal velocity condition that must be applied more carefully than the universal slip conditions. The wall nodes are located at a half of the lattice spacing Δ from the immediate neighboring nodes as shown on Fig. 8. The first layer of nodes along the wall are assigned a slip velocity given by (22b), after the tangential wall electric field has been computed from the Laplace solver. The only exception to this rule occurs at the corner node. The ejecting velocity u_c is assigned to the first node diagonally away from the corner. As seen in Fig. 2, the derived ejecting slip velocity u_c is at a distance δ (Debye layer thickness) from the tip and tangential on either sides of the wedge. The actual ejecting velocity assigned to the corner node located at a distance $\Delta/\sqrt{2}$ from the corner is not u_c but u_c^{node} such that the net ejecting flow condition is satisfied.

We expect the ejecting flow to be nearly irrotational flow near the corner just outside the Debye layer, as is the case of the classical outer linear electrokinetic flow. However, at a finite distance away, the vortices and back pressure will render it a viscous Stokes flow that is eventually dominated by the harmonic of (30). Exactly where the transition occurs depends on the ejecting velocity assigned to the corner node, which has yet to be specified. It depends on the local Reynolds number based on the channel width W and the assigned ejecting velocity.

Based on these arguments, the radial velocity should decay as r^{-1}, as is the case for a point source of inviscid flow in two dimensions. Hence, the appropriate ejecting velocity to be assigned to the corner node is

$$u_c^{\text{node}} = u_c \left(\frac{\delta}{(\pi-\alpha)(\Delta/\sqrt{2})} \right), \tag{33}$$

which results from flow rate balance at a radius of $\Delta/\sqrt{2}$ and assuming that the ejecting flow spans an angle of $(\pi-\alpha)/2$ on either sides of the ejecting line of symmetry as shown in Fig. 2. Its value depends on the grid spacing. In our simulations, Δ is held constant at the value of $0.01W$ and we then expect from (31) that the entrainment should be approximately $[(\pi-\alpha)/2\sqrt{2}]u_c^{\text{node}}\Delta$.

We impose the ejecting velocity of (29c) at the corner node as shown in Fig. 8, directed towards the outer corner. We have performed LBM flow simulation for different values of u_c^{node}. Hence, each of the solutions and flow profiles would correspond to different strengths of the corner singularity and field leakage effects. In the LBM simulation, a relaxation time constant of $\tau=1$ is used. It corresponds to a viscosity of $\mu=(2\tau-1)/6=\frac{1}{3}$ units as in LBM. The far-field velocity is given a small value of $u_o=0.001$. Since the width of the channel consists of 100 nodes, the Reynolds number of the flow is $\text{Re}=\rho u_o W/\mu=0.3$ where $\rho=1$ is the density of the fluid or particles at each node. The creeping flow condition described by the biharmonic equation is hence well approximated in the LBM simulation. Each simulation is run until a steady flow is established or for 10^4 time steps. Stream function of the flow is constructed from the obtained velocity fields at the end of simulation. The contours of stream lines are plotted in Figs. 9(a)–9(d) for different values of the corner ejecting velocities u_c^{node}. As the strength of the corner ejecting flow increases, the pair of vortices becomes prominent on either side of the corner. However, the upstream vortex is extremely weak and, even when it appears at high u_c^{node}, it is detached from the corner. The outer flow and higher-order harmonics seem to favor the back vortex. Nevertheless, entrainment of streamlines still occurs upstream and intensifies with increasing u_c^{node}, with or without a front vortex. The spiral aggregate of Fig. 1 resembles the streamlines around the back vortex in Fig. 9.

In Fig. 10(a), the normal velocity in the direction of diagonal is shown for several values of u_c^{node}. All of them decay as $r^{-(2\lambda+1)}=r^{-7/3}$ as in the dominant harmonic of the viscous Stokes flow in (30) for most of the intermediate region. For a 90° bend or wedge with $\alpha=\pi/4$, $\lambda=\pi/2(\pi-\alpha)=\frac{2}{3}$. However, in the vicinity of the corner it has a power law scaling of r^{-1} which is the solution for potential flow ejected radially in two dimensions from a point source, as we have speculated. The irrotational character of linear electrokinetic flow has been revoked by the ejecting flow near but not exactly at the corner due to field leakage. However, at the high ejecting flow, the corner flow remains a potential flow. The fraction of flow entrained is estimated from the value of stream function at a distance of $\frac{1}{10}$ of width normally away from the corner on the horizontal branch of the channel and the data is plotted in Fig. 10(b). It agrees with the theoretical prediction of (31) that the entrainment fraction is $u_c\delta/2u_oW$ or $(\pi-\alpha)u_c^{\text{node}}\Delta/2\sqrt{2}u_oW$, which are dimensional versions of (31).

If the ejecting velocity is weaker than the far-field electrokinetic flow, the short interval of potential flow seen in Fig. 10(a) may not exist. The ejecting flow is entirely Stokes flow and its velocity decays radially due to momentum loss

PROOF COPY 022212PHF

PROOF COPY 022212PHF

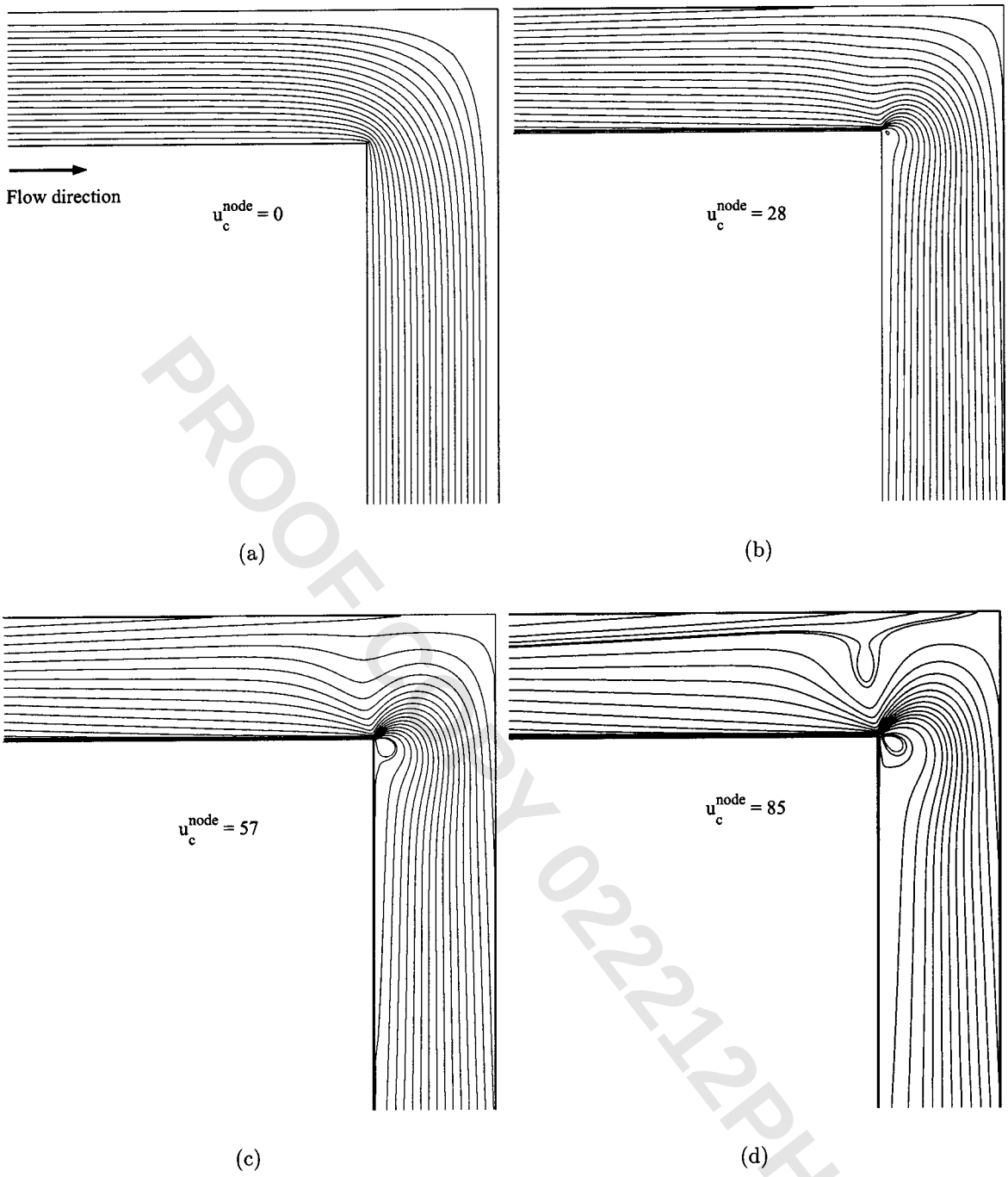

FIG. 9. Streamlines of electrokinetics flow in a channel with 90° bend obtained from LBM simulation for various strength of the corner ejecting flow. (a) $u_c^{\text{node}}=0$, with no field leakage effect, (b) $u_c^{\text{node}}=28$, (c) $u_c^{\text{node}}=57$, and (d) $u_c^{\text{node}}=85$. The far-field linear electrokinetic velocity is taken to be unity.

instead of the geometric effects on flow balance. In that case, the proper nodal ejecting velocity should be from the dominant Stokes flow scaling of (30) with a faster decay than (33),

$$u_c^{\text{node}}=\frac{u_c\beta}{2}\left(\frac{\Delta}{\delta}\right)^{\beta-1}, \tag{34}$$

where $\beta=-\pi/(\pi-\alpha)$. However, with such weak ejecting flow, there is insignificant entrainment and vortices do not appear. Correspondingly, the u_c^{node} used in Fig. 9 would correspond to atomically sharp corners if (34) is used. A good criterion to determine whether (33) or (34) to be used is to evaluate the ejection Reynolds number

$$\text{Re}_c=\frac{\rho_f u_c W}{\eta}. \tag{35}$$

If Re_c is much less than unity, (34) should be used. For a typical applied field of $E_o=100$ V/cm, Debye layer thickness of $\delta=50$ nm, and $\epsilon_w/\epsilon_f=\frac{1}{20}$, we estimate from (29b) and (35) for a 90° wedge ($\alpha=\pi/4$) in a channel of width 1 mm that Re_c exceeds unity when the radius of curvature r_c is

PROOF COPY 022212PHF

PROOF COPY 022212PHF

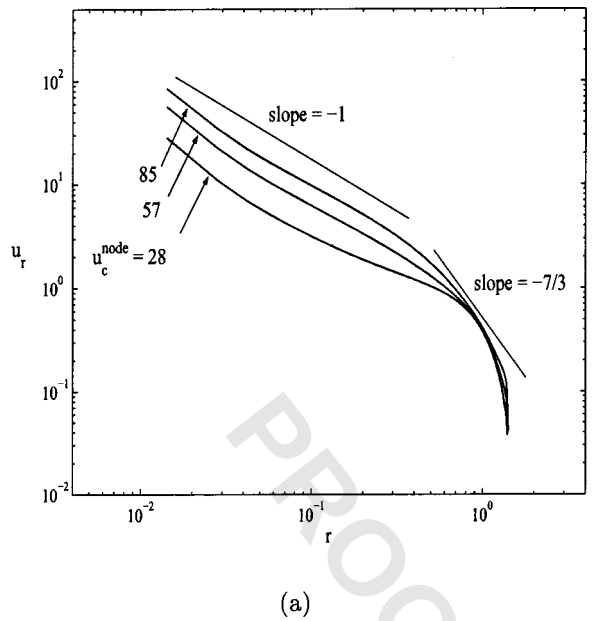

(a)

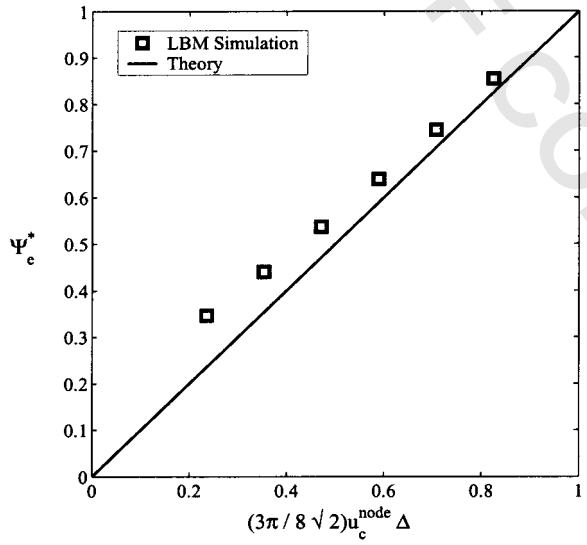

(b)

FIG. 10. (a) The decay of ejecting velocity away from the inner corner obeys the scalings of r^{-1} in the immediate neighborhood and $r^{-7/3}$ for the most of intermediate region. (b) Fraction of flow entrained to the corner plotted as a function of corner ejecting velocity. These data obtained from LBM simulation is approximately $2\alpha u_c^{node}\Delta/\sqrt{2}u_0 W$ as predicted by theory. The grid spacing is $\Delta = 0.01W$ with width $W = 1$.

below 100 nm. This critical roughness dimension approaches one micron for sharp wedges with α less than 10°. Submicron roughness is the rule for plasma etched channels in micro-channels, (see Fig. 1), particularly when silica is used. We hence expect (33) to be more relevant.

V. CONCLUSION

We have shown that electrokinetic flow past a wedge produces vortices if the channel wall has a finite dielectric permittivity. Due to the singularity and localized nature of normal field leakage, we have combined the effect of resultant opposing nonlinear slip velocities into an ejecting velocity at the corner. Hydrodynamic entrainment vortices are shown to exist on opposite sides of the wedge corner through local analysis and by numerical simulation. We have also implemented a multi-scale analysis and developed a simulation strategy. In the simulation approach, an effective boundary slip condition from our analysis is applied and the microhydrodynamics is simulated by a lattice Boltzmann method (LBM). The corner ejecting velocity arises from flow balance and must be implemented judiciously to the LBM code with (33). Unlike Moffat eddies[12] in pressure-driven flows at the outer corner, here nonlinear electrokinetic vortices occur at the inner corner. They are far more ubiquitous and their size and intensity increase with sharper corners, decreasing wedge angle, larger (ϵ_w/ϵ_f), larger electric fields, and smaller channel widths, as indicated by (29b) and (32). These vortices entrain proteins and colloids and induce aggregation at the inner corners but they can also be exploited to mix reagents—a valuable modification of the otherwise irrotational linear electrokinetic flow.

The electric field and velocity field singularities at the corner can also be removed by mechanisms other than finite tip curvature. We have neglected tangential ion fluxes in our theory. Such fluxes include convection to the tip, electromigration of ions to the tip, and diffusion away from the tip. The first two flux mechanisms act to enhance the singularity while diffusion, as usual, acts to regularize (smooth) the polarization around the tip. We expect convection contribution to be weak unless the polarized region extends far out of the Debye layer. Electromigration and diffusion, however, can balance around the tip to produce an effectively smoothed field which is not singular. A simple scaling argument indicates that this balance would produce a tangential Debye–Boltzmann distribution within a tip region of size $(RT/\mathrm{F})/E_c$ where E_c is a characteristic tangential field at the tip. We expect the tangential field at the radius of curvature r_c of 100 nm to be roughly 10^3 V/cm and this would produce a tangential Debye length scale of 250 nm, which is comparable to the expected dimension of r_c. Hence, tangential flux is negligible for a distance of r_c and larger away from the tip. This justifies our omission of the tangential flux from the theory.

ACKNOWLEDGMENT

This work is supported by an NSF-XYZ-on-a-Chip grant.

[1]K. V. Sharp, R. J. Adrian, J. G. Santiago, and J. I. Molho, "Liquid flows in microchannels," in *The MEMS Handbook*, edited by M. Gad-al-Hak (CRC, Boca Raton, FL, 2002).
[2]J. N. Israelachvilli, *Intermolecular and Surface Forces* (Academic, London, 1991).
[3]H. A. Pohl, *Dielectrophoresis* (Cambridge U.P., London, 1978).
[4]R. F. Probstein, *Physicochemical Hydrodynamics* (Wiley, New York, 1994).
[5]E. J. W. Verwey and J. T. G. Overbeek, *Theory of Stability of Lyophobic Colloids* (Elsevier, Amsterdam, 1948).
[6]Y. Ben and H.-C. Chang, "Nonlinear Smoluchowski slip velocity and micro-vortex generation," J. Fluid Mech. **461**, 229 (2002).

PROOF COPY 022212PHF

PROOF COPY 022212PHF

[7]R. P. Feynman, R. B. Leighton, and M. Sands, *The Feynman Lectures on Physics, Vol. 2. The Electromagnetic Field* (Addison-Wesley, Reading, MA, 1977).
[8]P. Sens and H. Isambert, ''Undulation instability of lipid membranes under an electric field,'' Phys. Rev. Lett. **88**, 128102 (2002).
[9]We use PDETOOL of MATLAB version 5.3.0.1083, copyright 1999, The Mathworks. For product information visit http://www.mathworks.com
[10]S. Chen and G. D. Doolen, ''Lattice Boltzmann method for fluid flows,'' Annu. Rev. Fluid Mech. **30**, 329 (1998).
[11]S. Hou, Q. Zou, S. Chen, G. D. Doolen, and C. C. Allen, ''Simulation of cavity flow by lattice Boltzmann method,'' J. Comput. Phys. **118**, 329 (1995).
[12]K. Moffat, ''Viscous and resistive eddies near a sharp corner,'' J. Fluid Mech. **18**, ■■■ (1964).

PROOF COPY 022212PHF

PROOF COPY 022212PHF